

Low-Rank + Sparse Decomposition (LR+SD) for EEG Artifact Removal

J. Gilles^a, T. Meyer^a, P.K. Douglas^b

^aDepartment of Mathematics, University of California, Los Angeles, 520 Portola Plaza, Los Angeles, CA 90095, USA

^bJane & Terry Semel Institute for Neuroscience & Human Behavior, David Geffen School of Medicine, University of California, Los Angeles, California, USA

Abstract

Concurrent EEG-fMRI recordings are advantageous over serial recordings, as they offer the ability to explore the relationship between both signals without the compounded effects of nonstationarity in the brain. Nonetheless, analysis of simultaneous recordings is challenging given that a number of noise sources are introduced into the EEG signal even after MR gradient artifact removal with balistocardiogram artifact being highly prominent. Here, we present an algorithm for automatically removing residual noise sources from the EEG signal in a single process using low rank + sparse decomposition (LR+SD). We apply this method to both experimental and simulated EEG data, where in the latter case the true EEG signature is known. The experimental data consisted of EEG data collected concurrently with fMRI (EEG-fMRI) as well as alone outside the scanning environment while subjects viewed Gabor flashes, a perceptual task known to produce event related power diminutions in the alpha spectral band. On the simulated data, the LR+SD method was able to recover the pure EEG signal and separate it from artifact with up to three EEG sources. On the experimental data, LR+SD was able to recover the diminution in alpha spectral power that follows light flashes in concurrent EEG-fMRI data, which was not detectable prior to artifact removal. At the group level, we found that the signal-to-noise ratio was increased 34% following LR+SD cleaning, as compared independent component analysis (ICA) in concurrently collected EEG-fMRI data. We anticipate that this method will be highly useful for analyzing simultaneously collected EEG-fMRI data, and downstream for exploring the coupling between these two modalities.

Keywords: EEG, Concurrent EEG-fMRI, balistocardiogram, artifact removal, robust, PCA, low rank, sparsity, sparse decomposition

1. Introduction

Simultaneous EEG-fMRI recordings are increasingly used to study the rich temporal dynamics of the human brain noninvasively. Each modality offers complementary benefits in signal detection: EEG scalp recordings provide high density temporal data yet resolves over diffuse spatial regions in the source domain, while fMRI signals provide high spatial precision, and yet evolve slowly due to temporally smoothed hemodynamics (Daunizeau et al., 2009). The idea of creating a principled method for EEG-fMRI fusion is highly attractive (Valdes-Sosa et al., 2009), particularly given its promise in localization of epileptic foci (R.Thornton et al., 2011; Grouiller et al., 2011). However, analysis of these multimodal data have proven quite challenging, given a number of artifacts introduced - particularly into the EEG signal - during concurrent recordings.

EEG recordings putatively reflect the superposition of electric dipoles associated with synchronous activity from neural populations measured at the scalp (Buzsáki et al., 2012; Dahne et al., 2013). When collected outside the

MR scanning environment, these signals are corrupted by a series of artifacts including: line noise (50/60 Hz electrical noise), electromyogram (EMG) activity, and electrooculogram (EOG) noise. In the case of simultaneous EEG-fMRI experiments, the artifacts are even more complicated. The most prominent signal contamination arises due to the switching of magnetic fields. However, a number of averaging based template-subtraction methods exist which are largely effective at removing this periodic gradient artifact (Goldman et al., 2002; Ritter and Villringer, 2006).

Although smaller in amplitude, a number of additional quasi-periodic artifacts cause electromagnetic interference in the MR environment that are not easily removed using template based methods. The ballistocardiogram (BCG), generated as EEG electrodes move due primarily to pulsatile head-rotation motion during the cardiac cycle (Mullinger et al., 2013), is particularly problematic (Srivastava et al., 2005), and presents broadly in the spectral frequencies of interest in EEG (0.5-25 Hz) (Debener et al., 2008). Similarly, the magnetic cryo-pump can induce noise with high trial-by-trial variability, and is therefore turned off typically during concurrent EEG-fMRI acquisition (Mullinger et al., 2013). The presence of these

Email addresses: jegilles@math.ucla.edu (J. Gilles), euphiab@gmail.com (T. Meyer), pamelita@ucla.edu (P.K. Douglas)

artifacts can dramatically change the spectral properties of the signal, and obscure ability to perform trial-by-trial analyses.

1.1. EEG Artifact Removal Techniques

Many artifact removal techniques have been developed in the last decade to address these issues. For instance, in Allen et al. (1998), the authors propose a template-based BCG artifact removal method called AAS (Average Artifact Subtraction). First, they detect timings when R peaks occur in the ECG (electrocardiogram) signal and extract several “small” portions of the EEG signal centered to these timings which are averaged to create a template for subtraction of the BCG artifact. In Allen et al. (2000), the authors combine the AAS method and an Adaptive Noise Cancellation (ANC) procedure synchronized with the slice-timing signal in order to remove residual artifacts. Independent component analysis (ICA) based blind source separation techniques have also been used for BCG removal (Makeig et al., 1996; Jung et al., 1998, 2000). Effectively, ICA decomposition of the N EEG channels is performed and the corrected EEGs are obtained by recomposing the ICA components without the “artifact components,” and the process of how a component is designated as artifact or not can be manual or automatic. In Mantini et al. (2007), the authors propose a method which combines AAS and ICA techniques to clean the EEG signals. A temporal principle component analysis (PCA) method has been used to create a series of artifact templates, termed optimal basis set (OBS) (Niazy et al., 2005), and has also been used in combination with ICA (Debener et al., 2007). In Zou et al. (2012), clustering is applied to IC components to separate the artifact components from the useful ones. In Sun et al. (2009), the authors adapt a blind source separation algorithm called Maximum Noise Fraction (MNF), originally developed for multispectral imaging, to remove the BCG artifact.

Another category of techniques is based on adaptive filtering methods. In Masterton et al. (2007), the authors record the BCG and body movements separately. Then they use an adaptive filtering technique called “Multi-Channel Recursive Least Square,” a particular case of Kalman filtering, to adaptively remove the recorded movements from the EEG signals. This approach seems to outperform AAS techniques but requires extra movement recordings. In Correa et al. (2007), the authors simulate the line noise and use extra recording of ECG and EOG as input of three adaptive filters. The first one remove the line noise, the second one the ECG artifact and the last one the EOG artifact. Each filter is a finite impulse response filter where their coefficients are continuously updated by a Least Mean Square algorithm. Nonetheless, most artifact removal methods generally require either a priori knowledge in the form of user identification of artifact components or an artifact template, which may be time consuming or unavailable.

Here, we introduce a new algorithm for removing artifact from EEG signals that uses low rank + sparse decomposition (LR+SD). To do so, we propose a mathematical model based on a reasonable experimental assumption that artifact components will be mathematically expressed differently than the data themselves. Importantly, this method obviates the need for any reference or template artifact signal. As such, the combined effects of many types of artifacts can be removed in a single decomposition without the need for manual identification of artifact components in the data. We assess the utility of this new algorithm first using simulated EEG data with a known solution. Next, we apply this method to real experimental EEG data collected concurrently in the scanner room with fMRI data while subjects performed a visual perception task. We then compare our novel LR+SD method to conventional ICA based artifact removal techniques to EEG data collected serially outside of the scanner on this same visual task.

2. Methods

2.1. Overview

Our method in brief is as follows. We first describe our simulated EEG data set with a known solution. We then describe our stimulus paradigm, our method for concurrent EEG-fMRI data collection, and our serially collected EEG data set collected outside of the MR scanning environment using the same stimulus paradigm. We used both in and out of scanner data for testing our novel artifact removal technique experimentally. We then describe our LR+SD method in detail, and methods used for comparing the performance of this algorithm to existing methods.

2.2. Simulated Dataset

In general, there is no ground truth EEG signal when data are empirical, making it difficult to assess the utility of artifact-removal algorithms. We therefore created a simulated dataset by using the free BESA (Brain Electrical Source Analysis) Simulator ¹ to generate “pure” EEG signals corrupted by known artifacts. We prepared two simulated datasets of varying complexity using forward modeling with a spherical head model. Data were simulated using the “Adult cr80” EEG sensor model, sampled at 125Hz over 10000 points. In dataset I, we simulated data for a single dipole source near the cortical surface in the visual region. In dataset II, three dipoles sources located in distributed brain areas were used to simulate data. A Hanning filter was applied to all simulated sources. For data set I, we simulated data for a 20 nAm sine wave at 10Hz occurring in the interval [15 – 17]s, located at $(-0.219, -0.646, 0.036)$ with orientation $(0.479, -0.336, -0.811)$ (visual cortex). In simulation II,

¹Available at http://www.besa.de/updates/besa_simulator/

the three sources included: one 4 nAm sine wave at 12Hz in the interval [5 – 10]s at position (−0.219, −0.646, 0.036) with orientation (0.479, −0.336, −0.811) (visual cortex), one 3 nAm sine wave at 6Hz in the interval [23 – 33]s at position (0.284, 0.644, 0.168) with orientation (−1, 0, 0) (frontal lobe) and a 5 nAm sine wave at 20Hz in the interval [53–56]s at position (−0.438, 0.05, 0.5) with orientation (1, 0, 0) (primary motor cortex). In order to add realistic noise to the data, we used ECG, EMG, and right and left EOG reference artifact recordings extracted from the free sample of the SHHS Polysomnography Database² (see Goldberger et al. (2000); Quan et al. (1997); Lind et al. (2003); Redline et al. (1998) for more information). These reference artifacts were normalized and added to the pure simulated EEGs using randomized mixing coefficients accordingly to a uniform distribution.

2.3. Experimental Data: Participants and Stimuli Design

A total of ten healthy individuals (ages 23-30, twelve male) without history of neurological disease were recruited to participate in this study, which was approved by the UCLA Institutional Review Board. Each individual provided written informed consent at the Staglin Center for Cognitive Neuroscience prior to participation in the study. The experiment consisted of concurrent EEG-fMRI data collection, followed by single modality EEG data collection outside the scanner suite.

Concurrent data was collected in a dimly lit MR scanner room while a subject passively viewed visual stimuli, presented via an MR projector screen. Stimuli consisted of Gabor element ‘flashes’ presented radially against a black background. A total of 140 flashes were presented to each subject for 500 msec each. We jittered the timing of the stimulus presentation with a minimum inter stimulus interval of 9 sec (mean 12.85 +/- 2.8 sec). We used a long ISI to allow plenty of time for the EEG alpha power to return to baseline following the flash stimulus. During the inter stimulus interval, subjects were asked to fixate on a low contrast small grey crosshair centered on the screen. We selected this task, as it has been shown to generate reproducible activations in functionally defined brain regions across both modalities. Light stimuli consistently elicit event related spectral perturbations (ERSPs) in EEG occipital channels (Huettel et al., 2004).

2.4. Data Acquisition: Concurrent EEG-fMRI and Single Modality EEG

Simultaneous EEG/ fMRI data were recorded using a high density 256-channel GES 300 Geodesic Sensor Net (Electrical Geodesics, Inc.) with an EEG sampling rate of 500 Hz, and TR of 1sec. MRI clock signals were synced with EEG data collection for subsequent MR artifact removal. Functional scans were acquired using 3-T Siemens

Trio MRI Scanner using echo planar imaging gradient-echo sequence with echo time (TE) of 25msec, repetition time of 1s, 6mm slices, 2mm gap, flip angle 90 degrees, with 3mm in-plane resolution, ascending acquisition. A high resolution structural image was collected using the magnetization-prepared rapid-acquisition gradient echo (MPRAGE) protocol (slice thickness 1.5mm, 1mm in plane resolution, flip angle 20 degrees, TE of 4.76, along with a T2 matched bandwidth scan to facilitate registration.

For comparison purposes, we also collected EEG data using this same visual task outside the scanner environment. These data were collected in a dimly lit copper shielded room using an EGI 256-channel Geodesic Sensor net with a 500 Hz sampling rate.

2.5. EEG Data Processing

Initial EEG data preprocessing and artifact detection was performed using tools available in EGI NetStation. EEG data first underwent MR artifact removal by subtracting an exponentially weighted moving average template, according to methods described in Goldman et al. (2002). Parameters for cleaning were chosen based on matching the frequency power spectrum with that of data collected out of scanner.

In order to compare our LR+SD method to established method, we performed either ICA or LR+SD on gradient-cleaned data. ICA based BCG removal was performed by applying the InfoMax ICA algorithm using Brain Analyzer v.2.0.2 software (Brain Products). Noise artifacts were then identified manually by visually inspecting the time series of the ICs as well as the power spectrum across the scalp channels, as was done in Mantini et al. (2007). Following either ICA or LR+SD cleaning, stimulus events were segmented 2 sec before and 10 sec after presentation of each stimulus. Subsequent artifact detection was accomplished using a gradient threshold of 400 μ V. If >20% of channels were marked as error, then that segment was excluded from further analysis, and if >30% of segments were marked as bad, then that particular subjects data was omitted for that task. Lastly, data were DC detrended across the duration of each segment.

3. Low Rank + Sparse Decomposition Method

We denote $\{\tilde{f}_i(k)\}_{i=1}^N$ the set of recorded EEG signals. The index i corresponds to the channel index, assuming we have a total of N electrodes distributed over the scalp. Moreover, we assume that each signal is recorded over K samples, i.e. $k \in \{1, \dots, K\}$. We consider J (unknown) artifacts, and will denote them $\{f_j^A(k)\}_{j=1}^J$ where the index j identifies different artifacts. The goal of the artifact removal procedure is then to retrieve cleaned EEG signals, $\{f_i(k)\}_{i=1}^N$.

²Available at <http://physionet.org/physiobank/database/shhpsgdb/>

In the proposed method we assume the following model: each recorded EEG channel is a linear combination of its cleaned version and the different artifacts. This model is equivalent to write

$$\tilde{f}_i(k) = f_i(k) + \sum_{j=1}^J a_{ij} f_j^A(k), \quad (1)$$

where the mixing coefficients a_{ij} are unknown. In the following, we use a matrix formalism to model the global processes. To do so, we cast each EEG and artifact channels as columns of $K \times N$ matrices:

$$\underbrace{\begin{pmatrix} | & | & & | \\ \tilde{f}_1 & \tilde{f}_2 & \dots & \tilde{f}_N \\ | & | & & | \end{pmatrix}}_{\tilde{F}} = \underbrace{\begin{pmatrix} | & | & & | \\ f_1 & f_2 & \dots & f_N \\ | & | & & | \end{pmatrix}}_F + \underbrace{\begin{pmatrix} | & | & & | \\ \tilde{f}_1^A & \tilde{f}_2^A & \dots & \tilde{f}_N^A \\ | & | & & | \end{pmatrix}}_{\tilde{F}^A}, \quad (2)$$

where $\tilde{f}_i^A(k) = \sum_{j=1}^J a_{ij} f_j^A(k)$. The matrix \tilde{F} contains all recorded EEG channels, F the wanted cleaned EEG signals and \tilde{F}^A contains the mixing of all artifacts. The latter can be written as $\tilde{F}^A = \sum_{j=1}^J F_j^A$ where

$$F_j^A = \begin{pmatrix} | & | & & | \\ a_{1j} \tilde{f}_j^A & a_{2j} \tilde{f}_j^A & \dots & a_{Nj} \tilde{f}_j^A \\ | & | & & | \end{pmatrix}. \quad (3)$$

The key to our method is to notice that each matrix F_j^A has its columns proportional to the same vector \tilde{f}_j^A implying that $\text{rank}(F_j^A) = 1$ and consequently $\text{rank}(\tilde{F}^A) \leq J$. Otherwise, the matrix F should contain events resulting from “true” EEG data. In our case, we focus on event related spectral perturbations (ERSPs), which occur at specific times and affect a limited number of electrodes. Therefore, it is reasonable to assume that F is a sparse matrix. Thus the artifact removal problem is equivalent to performing a low-rank + sparse decomposition of \tilde{F} . The resulting sparse component therefore corresponds to the cleaned EEG signals. Such decomposition can be done by solving the following minimization problem:

$$(F, F^A) = \arg \min \|F^A\|_* + \lambda \|F\|_1 \quad (4)$$

such that $\tilde{F} = F + F^A$,

where $\|\cdot\|_*$ denotes the nuclear norm of a matrix (i.e. the sum of its singular values), $\|\cdot\|_1$ denotes the sum of the absolute value of the matrix entries and λ is a positive parameter allowing us to control the rank of F^A . Such model, also called Robust PCA, was actively studied in the mathematics community, see for example Cai et al. (2008); Candès et al. (2009); Lin et al. (2009). In our experiments

we adopt the algorithm presented in³ Lin et al. (2009). For artifact removal of the empirical data, the regularization parameter was selected by running a sweep across all possible ranks for a test subject. The selected regularization parameter was then applied to the remaining subjects.

Upon publication, all code developed for this project will be available on the NITRC repository⁴.

4. Results

The Time-Frequency representation (TFR) is widely used to visualize how the energy in different spectral bands is evolving with respect to some stimuli. In this section, we use the TFR, computed via a continuous wavelet transform (CWT) using the Morlet wavelet, to assess the efficiency of the proposed method.

4.1. Results on Simulated EEG

In this section we illustrate the results obtained from applying low-rank + sparse decomposition (LR+SD) to the simulated datasets. In this case, we know the “true” EEGs and artifacts so our goal is to check if the proposed method is capable of retrieving both TFRs from the raw signals. Figure 1 shows the TFRs for the case of a single source. The TFRs corresponding to the pure and artifact signals are depicted in the two upper right plots while the TFR obtained from the raw EEGs (pure EEGs mixed with pure artifacts) is given on the upper left plot. Notice that the time-frequency energy corresponding to pure EEGs is nearly undetectable due to the artifact energy. The second row shows TFRs obtained from LR+SD.

The second dataset contains multiple events at different times and in different area of the brain. Figure 2 illustrates the obtained results (with the same plot layout as described for the single source case) from an electrode close to the activation areas. The signatures of each event are not visible in the raw EEGs’ TFRs yet they are clearly visible in the sparse component.

In both the single and multiple source experiments the regularization parameter λ had value $5 \cdot 10^{-3}$ which resulted in ranks of 4 and 5 for the low-rank artifact components, respectively. The proposed method shows excellent results in separating the artifact parts from the EEG signals of interest.

4.2. Results on Concurrent EEG-fMRI Acquisitions

Group level ERSF results for LR+SD artifact removal of our experimental data are summarized and compared to ICA artifact removal as well as out of scanner data in Figure 3(a-d). Signal-to-noise ratio (SNR) was computed by calculating the ratio of the maximum absolute signal diminution in alpha power from 0 to 500 msec following

³Matlab implementation available at http://perception.cs1.illinois.edu/matrix-rank/Files/exact_alm_rPCA.zip

⁴At <http://www.nitrc.org>

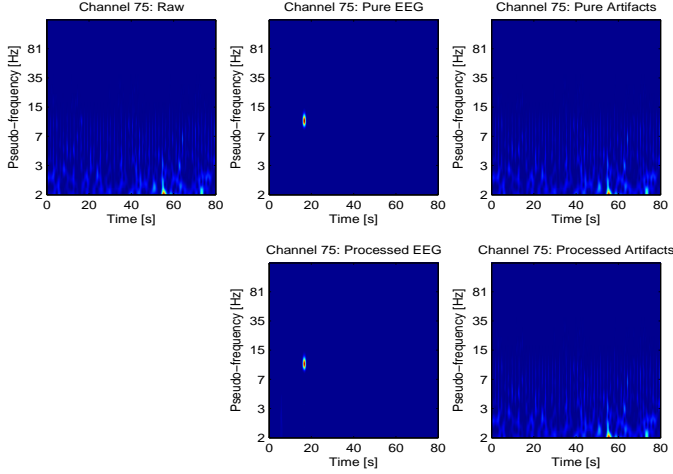


Figure 1: Simulated Data Set I. A single dipole source located close to an occipital electrode channel is mixed with artifacts. (Top row) TFR of the original simulated raw data corrupted by artifact (left), the true EEG data alone (middle), and artifact alone (right). (Bottom Panel) TFR of LR+SD results, which separates the cleaned EEG (left) from artifact (right). Values are normalized to maximum for each display.

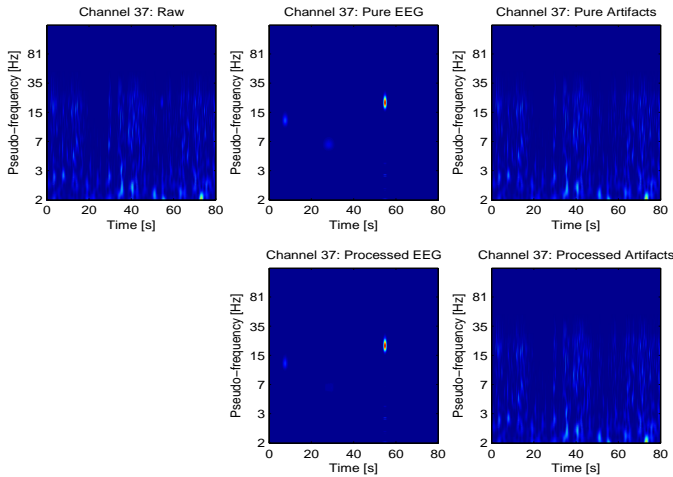


Figure 2: Simulated Data Set II. Three sources measured with an electrode located close to the primary motor cortex (source 3). (Top Panel) CWT of original simulated data consisting of three dipole sources corrupted by ECG, EMG and right and left EOG template artifacts (left), the true EEG data alone (middle), and artifact alone (right). (Bottom Panel) LR+SD result TFRs separating the cleaned EEG (left) from artifact (right). Values are normalized to maximum for each display.

stimulus presentation to the standard deviation of alpha power from the following 1000msec post stimulus. SNR was 8.5, 11.4, and 15.2 for ICA, LR+SD, and out of scanner data respectively. Figure 3(d) shows group level alpha spectral EEG data projected topographically for pre-stimulus (-250 msec), ERSP (50msec), and post stimulus (500 msec), with timings with respect to the stimulus occurring at time equal to zero.

Figure 4 shows single-patient alpha power averaged over all stimuli for a window of 2sec pre stimulus to 8sec post. The raw data is shown in comparison with the sparse

component from LR+SD and ICA using an average of the time-frequency intensity over alpha band frequencies. The strength at the specific frequency of 10Hz with bounds of one standard deviation is also shown for each dataset.

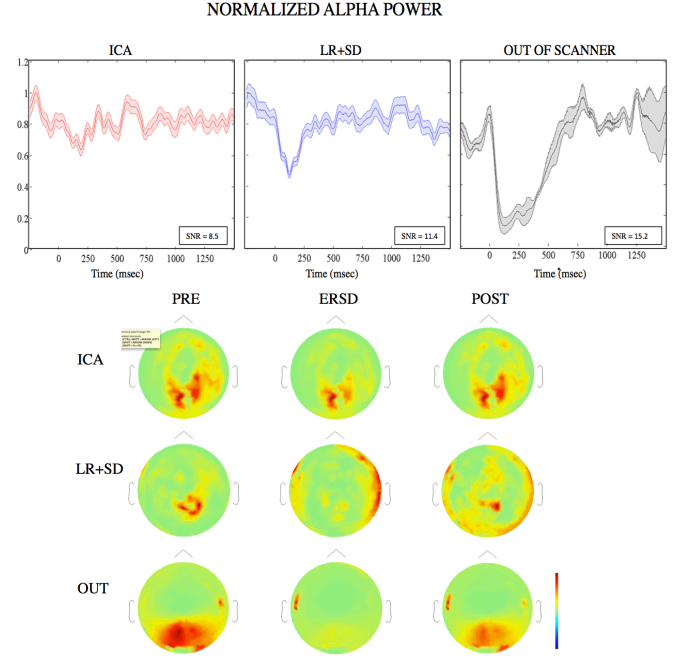


Figure 3: Group Level Results comparing independent component analysis (ICA) and LR+SD based cleaning to EEG data collected outside of the MR scanner environment. (TOP PANEL) Normalized Alpha Power time courses derived from the ocular EEG channel averaged across all subjects plotted with mean \pm SEM for ICA, LR+SD and Outside Scanner Results. Signal-to-Noise ratios are shown in the lower left corner for each result with the stimulus occurring at time equal to zero. (LOWER PANEL) Group level alpha power results projected topographically for 500msec prior to stimulus onset (PRE), 50 msec following stimulus onset (ERSD), and 500msec following stimulus onset (POST).

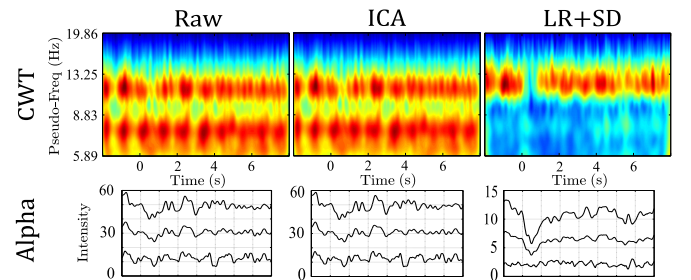


Figure 4: Single-subject alpha band TFR averaged over stimuli. Columns denote (left) the raw MRI signal, (center) the ICA-cleaned signal (right) the sparse component from LR+SD. For each dataset is shown (top row) TFR over a frequency range about the alpha band and (bottom row) the signal strength at 10Hz with single standard deviation bounds.

5. Discussion

In the present paper, we introduce a new method for removing artifacts from EEG signals, which decomposes data into the sum of two matrices: a sparse matrix representing the cleaned data, and a low-rank matrix, which corresponds to the artifact portion of the data. We applied this algorithm to remove artifact from two forms of data. In the first, we used simulated data where the pure EEG data was known, and corrupted by the addition of a series of canonical artifacts to the data using a randomized mixing matrix. In the second set of data, we applied LR+SD to empirical EEG data collected concurrently with MRI data.

Overall, LR+SD appeared effective on each of the two forms of event related data. The LR+SD algorithm was very effective at separating artifact from the pure EEG signal in our simulated data set with up to three true EEG sources. Our method also recovered the diminution in alpha power following a subject viewing a Gabor light flash, and improved the signal to noise ratio of detecting this ERSP by 34%. The LR+SD signal was clearly not as robust as the data collected out of scanner. Visually, the diminution in alpha power became apparent upon inspection following LR+SD in topographic projections of the data as well as at the single channel sensor level on the scalp.

6. Examining BCG Removal & Sparsity

Topographically, the BCG artifact is both non-uniform and dynamic. Its complex signature is thought to derive primarily from three key origins each with distinct R-wave latencies: pulse-driven head rotation, the Hall effect due to pulsatile blood flow, and pulsatile expansion of the scalp (Mullinger et al., 2013). If the BCG artifact was spatially static, it is possible that channel by channel template based methods may be adequate for its removal. However, the non stationary nature of the BCG makes its characterization and removal more complicated. Categorically, the pulse-driven head rotation appears to contribute most prominently to the amplitude of the artifact signal (Mullinger et al., 2013); however, the artifact, despite its origin, appears to be reflected in nearly all channels to varying degrees.

Overall, the LR+SD algorithm is quite similar to the robust PCA algorithm, which relies on a number of assumptions about the data. Specifically, it is assumed that the data events themselves are sparsely represented in the time domain. Artifacts are conversely assumed to be broadly distributed at the channel level across the scalp, which appears to be a relevant assumption given what has been observed about the distribution of EEG artifacts, mentioned above, thus far.

Results using ICA for artifact removal of concurrent EEG-fMRI have varied (Mantini et al., 2007; Eichele et al., 2005). Interestingly, the BCG artifact and its topographic

variability appear to be more problematic when experiments are carried out at higher MR field strengths. Results using ICA as a method for BCG artifact removal at 1.5T were initially quite promising (Mantini et al., 2007; Eichele et al., 2005). However, ICA has been shown to fail at 3T (Debener et al., 2008), the field strength used in the present study. It is possible that the larger magnitude artifact at higher field strength amplifies subtleties of the artifact that are subsequently split across components. Compared to ICA, LR+SD cleaning appeared to significantly improve the SNR of detectable ERSPs by controlling the rank of the artifact matrix.

In each of these data sets, the events occurred in temporally distinct time points relative to the data segment or epoch, making the sparsity assumption in the temporal domain relevant. Further, the ERSPs for the experimental data were measured across a dense 256 electrode net, and voltage fluctuations due to flash stimuli in channels located at large spatial distances from occipital electrodes is likely quite minimal. In this sense, the data of interest were also represented across a sparse number of channels. Further work is needed to characterize the conditions under which this sparsity assumption holds. For example, it is unclear how well this algorithm would perform when the signal of interest is continuously present across distributed electrodes, as might be the case when examining default mode network activity (Biswal et al., 1995).

It is also interesting to note that, after optimization, we found that setting our regularization parameter to rank 25 was effective at isolating BCG artifact. Lower ranks were ineffective at isolating the BCG noise, due to the complexity of the BCG signal itself. In the clinical setting, the ECG signal is often low-pass filtered and gross changes of its signature (e.g. ST segment elevation) are examined. However, lower amplitude changes in higher frequencies of the ECG exist and have been shown to correlate with cardiac ischemia (Schlegel et al., 2004) even up to 250Hz (Douglas et al., 2006). Given this broad spectral signature, it is unsurprising that more than a few sparse components were required to capture the artifact signals. In our online supplemental results, we provide a video “sweep,” illustrating how the low rank matrix, thought to reflect BCG and other artifacts, and sparse matrix, thought to reflect the data, components vary according to our regularization parameter value (see Supplemental).

7. Conclusions and Future Work

In this paper, we demonstrate that LR+SD worked quite well on event related data that was either simulated or empirical. One of the strengths of this method is that it eliminates the need for burdensome manual examination of components, and expert used decisions required to determine whether a given component is noise or part of the data themselves. This process, as may be the case when using ICA based artifact removal, can also vary across users. LR+SD provides an automatic method for parsing data

and artifact into separate groups, with the need to tune only one regularization parameter. Nonetheless, the SNR of data post LR+SD was still less than that of data collected outside the scanning environment. Future work may include applying this algorithm in combination with temporal kernel methods (e.g. Biessmann et al. (2010)) to effectively map the dynamic artifact to a stationary reference frame, and consider additional types of event related neuroimaging data that are corrupted by distributed artifact effects.

8. Acknowledgements

The authors want to thank the Keck Foundation for their support.

References

- Allen, P.J., Josephs, O., Turner, R., 2000. A method for removing imaging artifact from continuous eeg recorded during functional mri. *NeuroImage* 12, 230–239.
- Allen, P.J., Polizzi, G., Krakow, K., Fish, D.R., Lemieux, L., 1998. Identification of EEG events in the MR scanner: the problem of pulse artifact and a method for its subtraction. *NeuroImage* 8, 229–239.
- Biessmann, F., Meinecke, C., Gretton, A., Rauch, A., Rainer, G., Logothetis, N., Muller, K., 2010. Temporal kernel cca and its application in multimodal neuronal data analysis. *Machine Learning* 79, 5–27.
- Biswal, B., Yetkin, F., Haughton, V., Hyde, J., 1995. Functional connectivity in the motor cortex of resting human brain using echo-planar mri. *Magn Reson Med* 34(4), 537–541.
- Buzsáki, G., Anastassiou, C., Koch, C., 2012. The origin of extracellular fields and currents — eeg, ecog, lfp and spikes. *Nature Reviews Neuroscience* 13(6), 407–420.
- Cai, J.F., Candès, E., Shen, Z., 2008. A singular value thresholding algorithm for matrix completion. *SIAM Journal on Optimization* 20, 1956–1982.
- Candès, E., Li, X., Ma, Y., Wright, J., 2009. Robust principal component analysis. *Journal of the ACM* 58, 1–37.
- Correa, A.G., Laciari, E., Patiño, H.D., Valentinuzzi, M.E., 2007. Artifact removal from EEG signals using adaptive filters in cascade, in: 16th Argentine Bioengineering Congress and the 5th Conference of Clinical Engineering.
- Dahne, S., Biessman, F., Meinecke, F., Mehnert, J., Fazli, S., Muller, K., 2013. Integration of multivariate data streams with bandpower signals. *IEEE Transactions on Multimedia* 15(5), 1001–1013.
- Daunizeau, J., Laufs, H., Friston, K., 2009. Eeg-fmri information fusion: Biophysics and data analysis, in: Mulert, C., Lemieux, L. (Eds.), *EEG-fMRI*. Springer Press. volume 1, pp. 511–526.
- Debener, S., Mullinger, K., Niazy, R., Bowtell, R., 2008. Properties of the ballistocardiogram artifact as revealed by eeg recordings at 1.5, 3, and 7t static magnetic field strength. *Int J Psychophysiol* 67(3), 189–99.
- Debener, S., Strobel, A., Sorger, B., Peters, J., Kranczioch, C., Engel, A., Goebel, R., 2007. Improved quality of auditory event-related potentials recorded simultaneously with 3-t fmri: removal of the ballistocardiogram artefact. *NeuroImage* 34(2), 587–97.
- Douglas, P., Batdorf, N., Evans, R., Feiveson, A., Arenare, B., Schlegel, T., 2006. Temporal and postural variation of 12-lead high-frequency qrs electrocardiographic signals in asymptomatic individuals. *J Electrocardiol* 39(3), 259–265.
- Eichele, T., Specht, K., Moosmann, M., Jongsma, M., Quiroga, R., Nordby, H., Hugdahl, K., 2005. Assessing the spatiotemporal evolution of neuronal activation with single-trial event-related potentials and functional mri. *PNAS* 102(49), 17798–803.
- Goldberger, A.L., Amaral, L.A.N., Glass, L., Hausdorff, J.M., Ivanov, P.C., Mark, R.G., Mietus, J.E., Moody, G.B., Peng, C.K., Stanley, H., 2000. PhysioBank, PhysioToolkit, and PhysioNet: Components of a new research resource for complex physiologic signals. *Circulation* 101, e215–e220.
- Goldman, R., Stern, J., Engel, J., Cohen, M., 2002. Simultaneous eeg and fmri of the alpha rhythm. *Neuroreport* 13(18), 2487–2492.
- Grouiller, F., Thornton, R., Groening, K., Spinelli, L., Duncan, J., Schaller, K., Siniatchin, M., Lemieux, L., Seeck, M., Michel, C.M., Vulliemoz, S., 2011. With or without spikes: localization of focal epileptic activity by simultaneous electroencephalography and functional magnetic resonance imaging. *Brain* 134(10), 2867–2886.
- Huettel, S., McKeown, M., Song, A., Hart, S., Spencer, D., Allison, T., McCarthy, G., 2004. Linking hemodynamic and electrophysiological measures of brain activity: evidence from functional mri and intracranial field potentials. *Cerebral Cortex* 14(2), 165–173.
- Jung, T.P., Humphries, C., Lee, T.W., Makeig, S., McKeown, M.J., Iragui, V., Sejnowski, T.J., 1998. Removing electroencephalographic artifacts : Comparison between ICA and PCA. *Neural Networks for Signal Processing VIII*, 63–72.
- Jung, T.P., Makeig, S., Humphries, C., Lee, T.W., McKeown, M.J., Iragui, V., Sejnowski, T.J., 2000. Removing electroencephalographic artifacts by blind source separation. *Psychophysiology* 37, 163–178.
- Lin, Z., Chen, M., Wu, L., Ma, Y., 2009. The Augmented Lagrange Multiplier Method for Exact Recovery of Corrupted Low-Rank Matrices. Technical Report. University of Illinois at Urbana-Champaign. UILU-ENG-09-2215, arXiv:1009.5055v2.
- Lind, B., Goodwin, J., Hill, J., Ali, T., Redline, S., Quan, S., 2003. Recruitment of healthy adults into a study of overnight sleep monitoring in the home: experience of The Sleep Heart Health Study. *Sleep Breath* 7, 13–24.
- Makeig, S., Bell, A.J., Jung, T.P., Sejnowski, T.J., 1996. Independent Component Analysis of Electroencephalographic data, in: Touretzky, D., Mozer, M., Hasselmo, M. (Eds.), *Advances in Neural Information Processing Systems*. MIT Press. volume 8, pp. 145–151.
- Mantini, D., Perrucci, M., Cugini, S., Ferretti, A., Romani, G., Gratta, C.D., 2007. Complete artifact removal for eeg recorded during continuous fMRI using independent component analysis. *NeuroImage* 34, 598–607.
- Masterton, R.A., Abbott, D.F., Fleming, S.W., Jackson, G.D., 2007. Measurement and reduction of motion and ballistocardiogram artefacts from simultaneous EEG and fMRI recordings. *NeuroImage* 37, 202–211.
- Mullinger, K., Havelhand, J., Bowtell, R., 2013. Identifying the sources of the pulse artifact in eeg recordings made inside the mri scanner. *NeuroImage* 71(1), 75–83.
- Niazy, R., Beckmann, C., Iannetti, G., Brady, J., Smith, S., 2005. Removal of fmri environment artifacts from eeg data using optimal basis sets. *NeuroImage* 28(3), 720–737.
- Quan, S., Howard, B., Iber, C., Kiley, J., Nieto, F., O’Connor, G., Rapoport, D., Redline, S., Robbins, J., JM, S., Wahl, P., 1997. The Sleep Heart Health Study: design, rationale, and methods. *Sleep* 20, 1077–1085.
- Redline, S., Sander, M., Lind, B., Quan, S., Iber, C., Gottlieb, D., Bonekat, W., Rapoport, D., Smith, P., Kiley, J., 1998. Methods for obtaining and analyzing unattended polysomnography data for a multicenter study. *Sleep* 21, 759–767.
- Ritter, P., Villringer, A., 2006. Simultaneous eeg-fmri. *Neuroscience and biobehavioral reviews* 30(6), 823–838.
- R.Thornton, Vulliemoz, S., Rodionov, R., Carmichael, D., Chaudhary, U., Diehl, B., Laufs, H., Vollmar, C., McEvoy, A., Walker, M., Bartolomei, F., Guye, M., Chauvel, P., Duncan, J., Lemieux, L., 2011. Epileptic networks in focal cortical dysplasia revealed using electroencephalography-functional magnetic resonance imaging. *NeuroImage* 70(5), 822–837.
- Schlegel, T., Kulecz, W., DePalma, J., Feiveson, A., Wilson, J., Rahman, M., Bungo, M., 2004. Real-time 12-lead high-frequency qrs electrocardiography for enhanced detection of myocardial ischemia and coronary artery disease. *Mayo Clinic Proceedings* 79(3), 339–

- Srivastava, G., Crottaz-Herbette, S., Lau, K., Glover, G., Menon, V., 2005. Ica-based procedures for removing ballistocardiogram artifacts from eeg data acquired in the mri scanner. *Neuroimage* 24(1), 50–60.
- Sun, L., Rieger, J., Hinrichs, H., 2009. Maximum noise fraction (MNF) transformation to remove ballistocardiographic artifacts in EEG signals recorded during fMRI scanning. *NeuroImage* 46, 144–153.
- Valdes-Sosa, P., Sanchez-Bornot, J., Sotero, R., Iturria-Medina, Y., Aleman-Gomez, Y., Bosch-Bayard, J., Ozaki, T., 2009. Model driven eeg/fmri fusion of brain oscillations. *Human Brain Mapping* 30(9), 2701–2721.
- Zou, Y., Jr., J.H., Jafari, R., 2012. Automatic EEG artifact removal based on ICA and hierarchical clustering, in: *2012 IEEE International Conference on Acoustics, Speech and Signal Processing (ICASSP)*, Kyoto. pp. 649–652.

Appendix A. Additional Simulation Data

We simulated an EEG signal using three sources mixed with multiple artifacts. The analysis of the resultant data can be performed on any particular electrode. In Figures A.5 and A.6 we demonstrate the same analysis as in Figure 2 but instead using, respectively, data from the simulated electrodes near the visual cortex and close to the frontal lobe area.

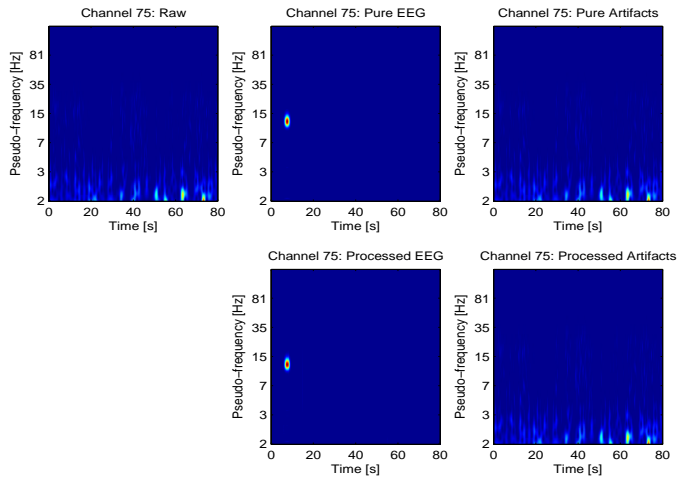


Figure A.5: Simulated Data Set II, second electrode. Three sources measured with an electrode located close to the visual cortex. (Top Panel) CWT of original simulated data consisting of three dipole sources corrupted by ECG, EMG and right and left EOG template artifacts (left), the true EEG data alone (middle), and artifact alone (right). (Bottom Panel) LR+SD result TFRs separating the cleaned EEG (left) from artifact (right). Values are normalized to maximum for each display.

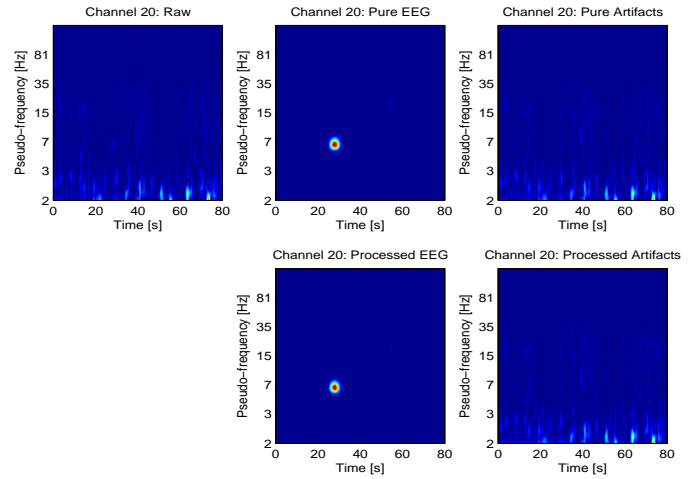


Figure A.6: Simulated Data Set II, third electrode. Three sources measured with an electrode located close to the frontal lobe area. (Top Panel) CWT of original simulated data consisting of three dipole sources corrupted by ECG, EMG and right and left EOG template artifacts (left), the true EEG data alone (middle), and artifact alone (right). (Bottom Panel) LR+SD result TFRs separating the cleaned EEG (left) from artifact (right). Values are normalized to maximum for each display.